BEAMFORMING STUDIES ON BASIC MODELS OF LOW-SPEED AXIAL FAN BLADE SECTIONS

E. Balla - J. Vad

Department of Fluid Mechanics (DFM), Faculty of Mechanical Engineering
Budapest University of Technology and Economics (BME)
Bertalan Lajos u. 4 - 6., H-1111 Budapest, Hungary. Email: balla@ara.bme.hu

ABSTRACT

The paper reports on establishing a beamforming dataset, relying on the phased array microphone (PAM) technique, on the broadband noise of rectilinear basic models of low-speed axial fan blade sections. A cambered plate profile is in the focus of the studies, in comparison with a flat plate and a traditional airfoil profile. At low Reynolds numbers, cambered plate blade sections have a potential to perform aerodynamically better than profiled airfoil sections. Thus, the established dataset aims at contributing to the design background of aerodynamically efficient, low-noise, low-Reynolds-number fans. The wind tunnel-PAM configuration enables the acoustic investigation over the plane being normal to the spanwise direction at midspan. An illustrative study on representative cases selected out of the dataset demonstrates the capabilities and limitations of the presently available experimental and evaluation method. Spatially simultaneously resolved information is presented on the signatures of systematically investigated classes of blade section noise.

KEYWORDS

beamforming, blade noise, cambered plate blade, low-speed axial fan, phased array microphone

NOMENCLATURE

C_D	section drag coefficient (2D)
C_L	section lift coefficient (2D)
c	chord length of blade section
d	maximum height of the camber line
d/c	relative curvature of the camber line
f_{mid}	middle frequency of third-octave frequency band
f_S	vortex shedding frequency
h	characteristic length scale for calculating St
Re	chord Reynolds number = cU/ν
SSL	source strength level (level of beamform source strength normalized by a reference value)
ΔSSL	subtractive source strength level (the effect of background noise removed)
St	vortex shedding Strouhal number = $f_S h/U$
s	span of model (length of stacking line)
t	model thickness
U	free-stream inlet velocity in x direction: along the longitudinal axis of the test section
x, y, z	coordinates. x: longitudinal (along the axis of the test section) / y: spanwise / z: vertical
α	angle of attack (between the chord line and the x direction)
ν	kinematic viscosity
Φ	flow coefficient (duct area-averaged axial velocity normalized by tip speed)
Ψ	total pressure coefficient (annulus mass-averaged total pressure rise divided by the dynamic pressure calculated with tip circumferential speed)

OPEN ACCESS
Downloaded from www.euroturbo.eu

Copyright © by the Authors

Abbreviations

BG background
LE leading edge
PAM phased array microphone
TE trailing edge

1. INTRODUCTION AND OBJECTIVES

Axial flow fans characterized by blade sections of chord Reynolds numbers of $Re \leq 10^5$ are termed herein as "low-Reynolds-number fans". Such fans are of relatively small size and/or rotor speed, e.g. cooling fans for computers (Huang, 2003) and for electric motors (Borges, 2012), or refrigerator fans (Gue et al., 2011).

Axial fans are often required to provide a prescribed flow rate and/or total pressure rise even at moderate diameter and/or rotor speed. These requirements are in accordance with the constraints of limited available space and/or speed – the latter being constrained e.g. by a directly-driving electric motor – in industrial applications. For these fans, the flow coefficient and the total pressure coefficient may extend over $\Phi \approx 0.4$ and $\Psi \approx 0.6$, incorporating operational ranges throttled significantly below the design flow rate (e.g. Corsini and Rispoli, 2004). Such fans are termed herein as "high-specific-performance fans". Their blade sections are often of high aerodynamic load – i.e. high lift coefficient –, high camber, and are often exposed to high α angles of attack.

Cambered plate blades of circular arc camber line are often applied in axial fans, enabling a relatively simple and low-cost manufacturing technique. A further reason for choosing cambered plate blades appears in low-Reynolds-number fan applications. For $Re \leq 10^5$, a cambered plate section may perform aerodynamically better than a profiled airfoil section. The potential benefits are the following: higher maximum lift coefficient C_L, and higher maximum lift-to-drag ratio C_L/C_D. Illustrative examples are given for such favourable trends by Carolus (2003), referring to Albring (1978). A comprehensive explanation is given herein on the basis of the experimental data and discussion by Mueller (1999) as well as by Yarusevych and Boutilier (2010). At low Reynolds numbers, laminar separation occurs near the leading edge (LE) of the blade section. Thinning the profile, i.e. sharpening the LE (profiled airfoil $\rightarrow$ cambered plate), tends to act as introducing a "turbulator" at the front part of the section, promoting the laminar-to-turbulent transition in the separated shear layer. By such means, the reattachment of the boundary layer over the suction side tends to be hastened. The thinner the profile, the earlier the boundary layer reattachment, i.e. the less extended the laminar separation bubble. The consequences of reattaching the boundary layer and moderating the extension of the separation bubble are as follows: improved suction effect, i.e. increased C_L, and narrowing the wake, i.e. decreased C_D. These trends are suggested by Yarusevich and Boutilier (2010), reducing the profile thickness from 0.25 c to 0.18 c (NACA 0025 $\rightarrow$ NACA 0018 airfoil). These favourable trends can be extrapolated for a cambered plate of thickness of some percent chord only. Due to the aforementioned benefits, cambered plates are considered also as wing profiles for micro-air vehicles (e.g. Mueller, 1999; Pelletier and Mueller, 2000).

The competitively high C_L and C_L / C_D values make the cambered plate blades especially beneficial in low-Reynolds-number, high-specific performance fans, if a reasonably good efficiency and/or moderate noise is a demand (e.g. Vad et al., 2014). The moderate C_D is associated with moderate aerodynamic loss. The fan noise strongly correlates with the global loss of the fan, as suggested in the Regenscheit method (VDI Richtlinie 3731, 1990; Carolus, 2003), and as confirmed by Daly (1992). The reduction of noise emitted by the axial fan is of great importance, especially in the view that the fans under discussion often operate in the vicinity of humans, such as computer processor cooling fans, cooling fans for electric motors in household devices, or refrigerator fans.

The above overview emphasizes the importance of experimentally studying both the aerodynamic and aeroacoustic behaviour of cambered plate blade sections, thus contributing to the background of designing low-Reynolds-number and/or high-specific performance fans. Such studies may also be adapted to the noise control of wings for micro-air vehicles (silent flight).

As suggested by Roger and Moreau (2010), detailed acoustic measurement data obtained for basic two-dimensional (2D), rectilinear models of blade sections can be adapted to rotating blades, by means of a spanwise segment splitting. Detailed acoustics measurements on a rectilinear airfoil, using multiple microphones, are reported by Padois et al. (2016). Beamforming, relying on the phased array microphone (PAM) technique, is a recently emerging methodology for obtaining spatially simultaneously resolved acoustic data on models of blade or wing sections. In beamforming the locus of the sound sources is estimated from the phase difference between the microphone signals of the PAM. The result of beamforming is displayed in source maps, which contain the strength levels of the sources. Further details on the fundamentals of the beamforming technique are available e.g. in Dougherty (2002) and Koop (2006). The papers by Hutcheson and Brook (2006), Geyer et al. (2012), Padois et al. (2015), Moreau and Doolan (2016), and Moreau et al. (2016) report on the PAM investigation of profiled rectilinear airfoils. These studies focus on high-speed fan and aerospace applications, and therefore, increased Reynolds numbers (exceeding $Re = 10^6$ in some cases) are characteristic.

Acoustic measurements on cambered plates are rarely published, and are focussed on externally blown flaps (e.g. Mckinzie and Burns, 1975). To the authors' best knowledge, the literature lacks in reporting any PAM-based acoustic measurements on rectilinear cambered plates with circular arc camber line, serving as models of axial fan blade sections. This is in accordance with the following fact. The recently emerging – and nowadays still relatively costly – PAM technique, as such, finds a number of turbomachinery-related applications in aerospace engineering (e.g. Horváth, 2015). It is still rare nowadays in low-speed fan-related applications (e.g. Minck et al., 2012; Herold and Sarradj, 2015; Benedek and Vad, 2016; Zenger et al., 2016).

In the view of the aforementioned lack, the objectives of the present paper, and the related potential for novelty content, are summarized in paragraphs 1) to 3) as follows.

1) Establishing a PAM-based dataset on representative, comparative basic models of low-speed axial fan blade sections. The models include a circular-arc cambered plate. The measurements offer a potential for adaption to low-Reynolds-number fans: $6 \cdot 10^4 \leq Re \leq 1.4 \cdot 10^5$. They offer a potential for adaption to high-specific-performance fans and/or to operating states throttled significantly below the design flow rate: $0° \leq \alpha \leq 30°$.

2) Establishing a primary evaluation methodology for the dataset. Presenting an illustrative case study, for demonstrating the capabilities and limitations of the reported experimental and evaluation method. On this basis, demands and guidelines for further improvement on the experimental campaign are outlined. The case study presents the acoustic features of the cambered plate, in qualitative comparison with other basic models, for the cases of $\alpha = 0°$, 10°, and 30°.

3) The wind tunnel-PAM setup enables the PAM investigation over the plane being normal to the spanwise direction at midspan. Thus, the aeroacoustic and aerodynamic features resolved in both wall-normal and chordwise direction can be correlated. As such, the noise associated with the thickened / separated blade boundary layer can be investigated in a lifelike manner. This is a supplement to the aforementioned PAM studies in the literature on blade or wing sections.

Three rectilinear basic blade section models are subjected to the PAM measurements. The circular arc cambered plate is acoustically compared to a flat plate and to a RAF6-E airfoil, for the following reasons. The flat plate is often taken as a reference case in computational and experimental aeroacoustics campaigns (e.g. Roger and Moreau, 2010; Sturm et al., 2015). RAF6-E is a popular profile of classic fan design, due to its easy-to-manufacture geometry (plain pressure surface). The aerodynamic and aeroacoustic features of a RAF6-E airfoil have been investigated e.g. by Vad et al. (2006).

For the primary evaluation presented in the paper, the maximum Reynolds number cases of $Re = 1.4 \cdot 10^5$ have been selected, in order to maximize the recognizable acoustic effects. Such choice is in accordance with the view that aeroacoustic phenomena are expected to exhibit higher levels with increasing mean-flow velocities (Roger and Moreau, 2010).

2. EXPERIMENTAL SETUP

The sketch of the measurement setup is shown in Figure 1. The measurements were carried out in the "Blackbird-2" wind tunnel at DFM. Details of the wind tunnel technique, including the properties of the generated flow, are described in Gulyás and Balczó (2014). The uncertainty of U has conservatively been estimated to ± 1.0 %. The non-uniformity of the inlet velocity is below 3% farther away from the endwall boundary layers, following the recommendation that the inlet velocity profile is to be as flat as possible (Roger and Moreau, 2010). The turbulence intensity in the inflow is 0.8 % for the presented cases. This is in accordance with the guideline that "clean inflow" is required for the experimental studies of vortex shedding noise and trailing edge (TE) noise – for the latter, turbulence rate below 1 % is recommended (Roger and Moreau, 2010).

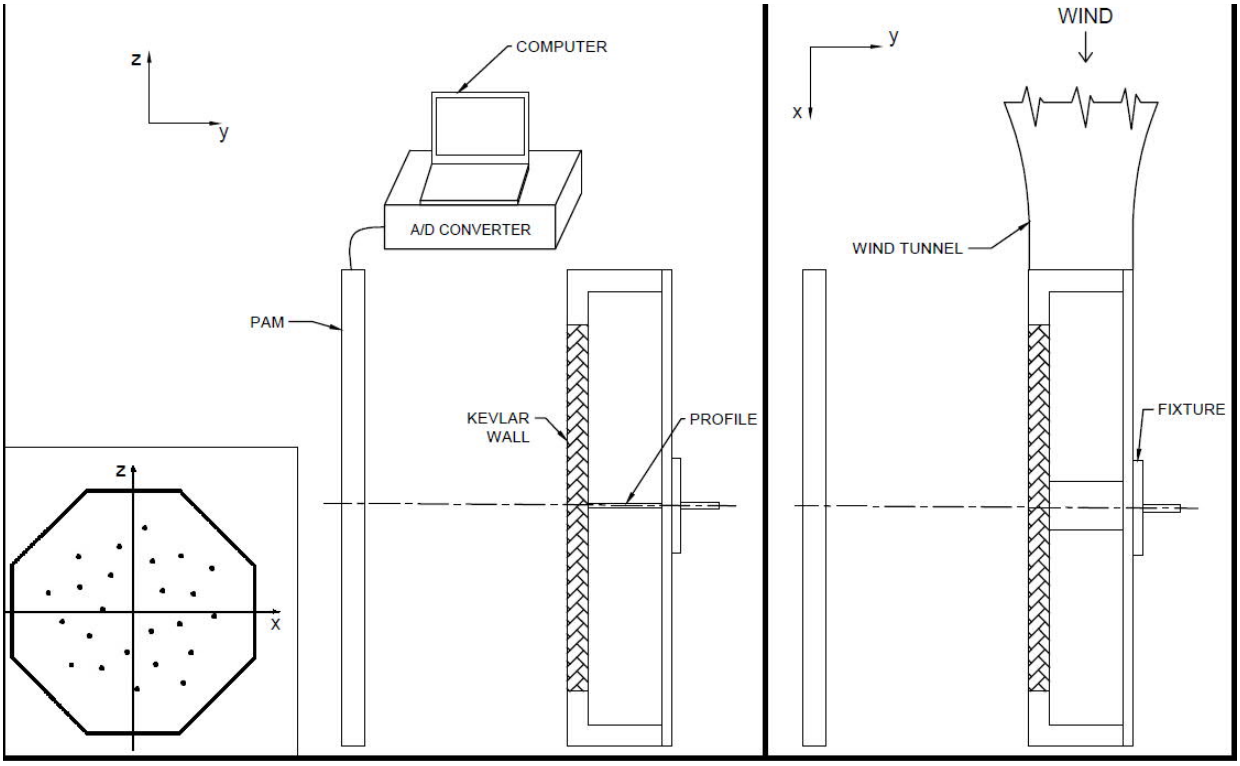

Figure 1. The experimental setup, from downstream (left) and upper (right) views. Bottom left: PAM octagonal plate, with sensor locations (not to scale with the other sketches).

Each blade section model – labelled as "profile" in Fig. 1 – was placed to the middle of the test section. A cylindrical handle has been attached to the profiles, with an axis being coincident with the stacking line of the profile. The blade section models were bounded by the wall of the test section from one side and by a Kevlar wall on the other side. The noise was measured by the PAM through the Kevlar wall. The distance between the midspan plane of the blade sections and the microphone array was set to 0.556 *m*. The stacking line of the blade section models has coincided with the PAM centreline, as indicated in the figure using dashed-dotted lines. The background (BG) noise was also measured: the profile was removed from the test section, and the noise of the empty wind tunnel was measured through the Kevlar wall.

At the present state of investigation, the mean flow deviation discussed by Roger and Moreau (2010) has been disregarded (conf. Balla and Vad, 2017). Therefore, α has been defined as the geometrical angle between the chord line and the longitudinal axis of the test section.

The noise was recorded by means of an OptiNav Inc. Array24 general purpose PAM. The aperture diameter of the PAM is 0.95 *m*. The duration of each measurement was 14 seconds. The analogous signals of the 24 microphones were amplified and converted to digital signals with an A/D converter. The signals were then saved by the data acquisition computer. The Beamform

Interactive plug-in of OptiNav was used to create the beamforming source maps.

Narrowband frequency domain beamforming was applied for various measurement durations and various normal-to-span measurement planes for the same experimental case. The PAM-based *SSL* results scattered within a range of ± 1 d*B* at 95% confidence level, for all cases examined. On this basis, the amplitude uncertainty has been estimated to ± 1 d*B*.

3. CASE STUDIES

The profiles – i.e. cross-sections – of the investigated three blade section models are shown in Figure 2. From this point onwards, the profiles will be referred to as "flat", "cambered", and "airfoil". The desired α can be set by rotating the fixture of the blade sections, at an uncertainty of ± 0.5°. The Mach number is 0.06, and thus, incompressible flow is considered. Further details on the measurement setup and the measurement conditions are given in Balla and Vad (2017).

The three α values discussed herein were selected on the basis of examining the $C_L(\alpha)$ and $C_D(\alpha)$ diagrams available for the three profiles in the classic literature (for "flat" and "cambered": Wallis, 1946; for "airfoil": Patterson, 1944). On this basis, the selected α values are representative for the following operational states of the blade sections: α = 0°: zero or moderate lift + nearly minimum drag; α = 10°: nearly maximum lift; α = 30°: deep stall. Considering the aerodynamic measurement data published by Mueller (1999) on flat and cambered plates, a 2D aerodynamic approach has been judged to be fair at the present level of evaluation (conf. Balla and Vad, 2017).

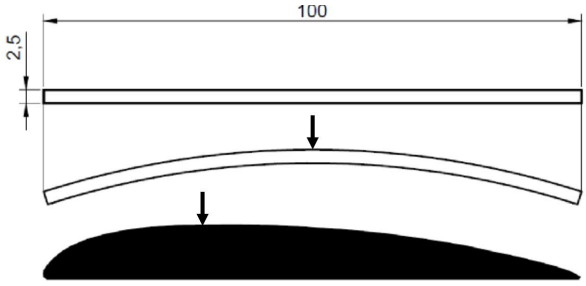

Profile	*c* [*mm*]	*s* [*mm*]	*t* [*mm*]	*d* [*mm*]
Flat	100	150	2.5	0
Cambered	100	150	2.5	8
Airfoil	100	150	10*	5
* maximum thickness				

Figure 2. The profiles: flat (top), cambered (middle), airfoil (bottom). The arrows indicate the location of *d*. The table presents the geometrical data of the models.

4. DETAILS OF DATA PROCESSING AND EVALUATION; NOISE SPECTRA

Beamforming was applied to the recorded sound data assigned to bands of 21.5 *Hz* width. Frequency domain beamforming was performed. In evaluation, the region of interest was confined to the vicinity of the profiles. The region extends half *c* upstream and one *c* downstream of the LE and TE, respectively. It extends twice *c* in lateral direction, with the profile being in the centre. The diagonal treatment of the cross spectral matrix was chosen to be optimized. Using this method, less information is lost than that using the "delete" method (Dougherty, 2016).

In order to get a general view on broadband noise, third-octave *SSL* spectra were derived (conf. Vad et al., 2006), as shown in the left column of Figure 3. In computing the spectra, the peak values of the beamform source strength were considered within each partial band of 21.5 *Hz* width. The phased-array technique serves herein not only for localizing the various sources of blade section noise, but also for making a distinction between the blade section noise and the background noise. The high level of BG noise (Fig. 3, left column) necessitates the application of background-noise subtraction (conf. Roger and Moreau, 2010), for a comprehensive evaluation of the spectra. Thus, subtractive (ΔSSL) spectra were obtained. ΔSSL has been computed as follows. The logarithmic *SSL* values were converted to source strength values for the noise of the actual blade section and the BG. Then, the latter was subtracted from the former. The result was then converted again to a logarithmic level.

The ΔSSL spectra, shown in the right column in Fig. 3, suggest the following approximate, generalized trends. The confirmation and comprehensive explanation of the observed trends and

phenomena, discussed in Sections 4 and 5, is a subject of future work, with involvement of detailed, concerted aeroacoustic-aerodynamic studies.

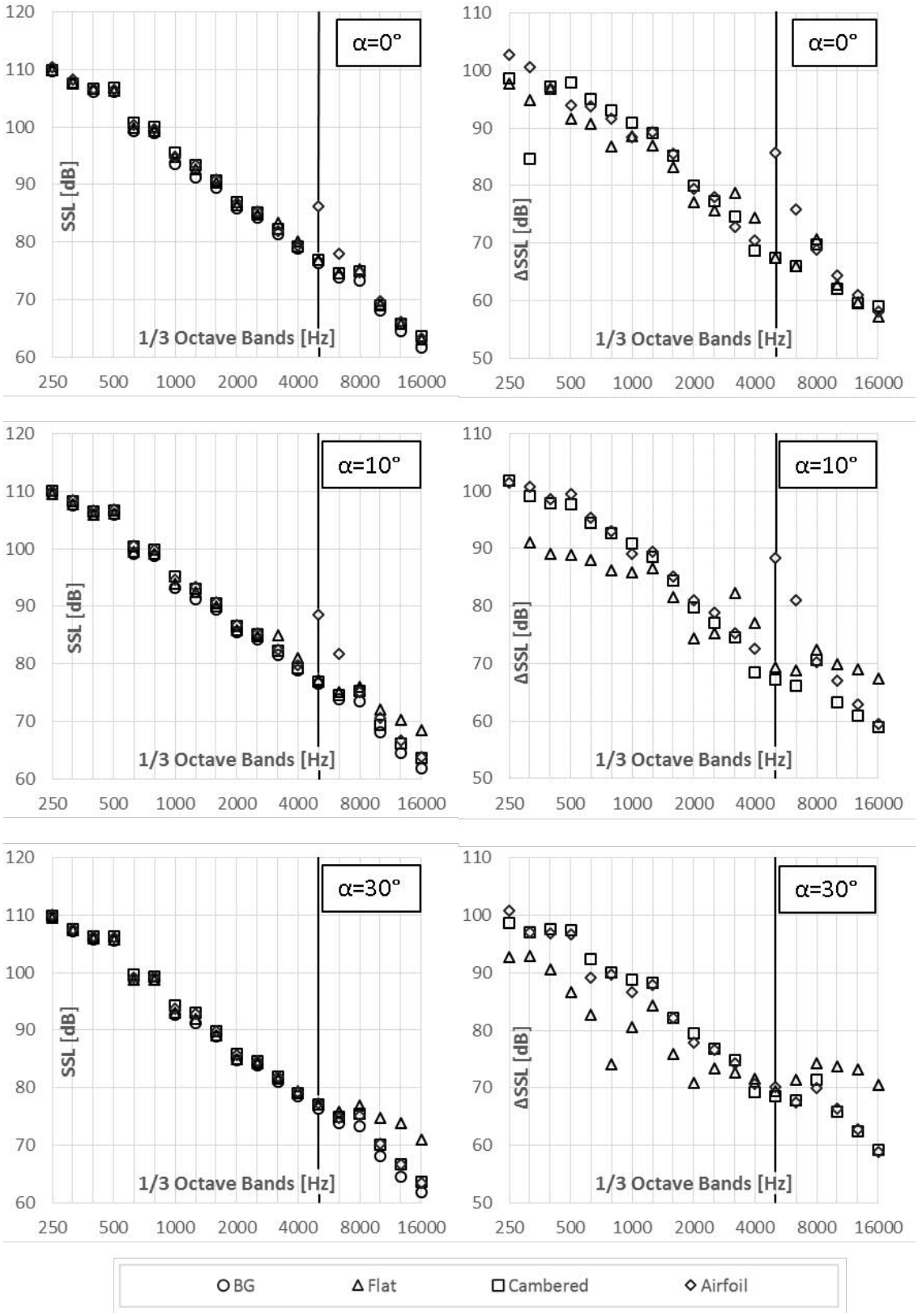

Figure 3. Original (left column) and subtractive (right column) third-octave noise spectra, for the frequency domain of f_{mid} = 0.25 to 16 k*Hz*. The bold vertical line indicates f_{mid} = 5 *kHz*.

Range of 0.5 to 3 kHz. For each α, ΔSSL of "cambered" and "airfoil" is higher than that of "flat". For $\alpha = 0°$ and $\alpha = 30°$, ΔSSL of "cambered" is higher than or equal to that of "airfoil". For $\alpha = 10°$, ΔSSL of "cambered" is lower than or equal to that of "airfoil".

Range of 3 to 8 kHz. For $\alpha = 0°$ and $\alpha = 10°$, ΔSSL of "cambered" is lower than or equal to that of "flat" and "airfoil", and outstandingly high ΔSSL values appear for "airfoil" at about 5 k*Hz*. For $\alpha = 30°$, such outstandingly high ΔSSL values disappear.

Range of 8 to 16 kHz. For $\alpha = 0°$ and $\alpha = 10°$, ΔSSL of "cambered" is lower than or equal to that of "airfoil". For $\alpha = 10°$ and $\alpha = 30°$, ΔSSL of "flat" is higher than that of "cambered" and "airfoil".

5. LOCALIZATION AND IDENTIFICATION OF NOISE SOURCES

This section aims at demonstrating the capabilities of the beamforming technique in localizing the sources of blade noise. Considering the works by Brooks et al. (1989), Carolus (2003), Staubs (2008), Yarusevych and Boutilier (2010), and Roger and Moreau (2010), the sources of broadband noise associated with the 2D blade section models are classified and briefly characterized herein as follows. The sources are listed in the presumed approximate sequence of their location, moving from the LE of the blade section toward the downstream direction.

a) *Turbulence-interaction noise.* It originates from the impingement of upstream turbulence. For aerodynamically non-compact cases, the source locates in the vicinity of the LE.

b) *Turbulent boundary layer noise.* It originates from the wall pressure fluctuation due to the turbulence in the boundary layer. It radiates within the entirety of the turbulent boundary layer.

c) *Separated flow noise.* It originates from boundary layer separation. For deep stall, the noise radiates from the entire chord. For mildly separated flow it dominates near the TE.

d) *Profile vortex-shedding noise.* It originates from coherent vortex shedding over the profile surface. The source extends from the wake toward the region upstream of the TE, within the possibly thickened / separated / reattached suction side boundary layer.

e) *Trailing-edge noise.* It is due to the scattering of the turbulence in an attached boundary layer, at the TE, as sound. The source is confined to the vicinity of the TE.

f) *Blunt trailing edge vortex-shedding noise.* It originates from coherent vortex shedding from the blunt TE. The source is confined to the region downstream of the TE.

Staubs (2008) and Roger and Moreau (2010) cite references and present their own studies on turbulence-interaction noise. In these references, the turbulence intensity varies between 4 to 6 %. Since the turbulence intensity is much less in the cases reported herein (0.8 %), the turbulence-interaction noise has been presumed negligible. Thus, sources b) to f) are discussed herein.

5.1. General interpretation on noise sources above 5 k *Hz*

Fig.3 suggests pronounced departures between the spectra above 5 k *Hz*. On this basis, it has been judged reasonable to start the discussion on spatially resolved data with a generalized interpretation in the range above 5 k*Hz*. Figure 4 shows the loci of representative sets of *SSL* peak values of the partial frequency bands of 21.5 *Hz* width, above 5 k*Hz*. The profiles are represented with their chord line in the figure. The rectangular region for presenting the loci of the peaks has arbitrarily been defined as follows. i) The longitudinal axis of the region is the bisector of the angle α, thus making an angle of $\alpha/2$ with the x axis. ii) The length of the region is c. iii) The width of the region is twice the α–dependent height of the projection of the profile to the vertical $[y,z]$ plane. The observations are summarized as follows.

$\alpha = 0°$. The peaks are located either close downstream of the LE at about 0.2 to 0.3 c, or at the vicinity of the TE. The former group is assumed to be related to the turbulent boundary layer noise, provoked presumably by laminar-to-turbulent transition. The latter group is assumed to be related to turbulent boundary layer noise and / or trailing-edge noise and / or vortex-shedding noise.

$\alpha = 10°$. 1) For "flat", peaks close downstream of the LE are still present, being closer to the

LE than for the $\alpha = 0°$ case. Such peaks cannot be observed for "cambered" and "airfoil". The peaks for "flat" are assumed to be related to the turbulent boundary layer noise, rising more upstream than for the $\alpha = 0°$ case, due to the higher angle of attack, and to the resultant more intense turbulence. For the curved suction surfaces of "cambered" and "airfoil", the near-LE part of the profiles is better aligned with the inflow direction at $\alpha = 10°$ than at $\alpha = 0°$. As a result, the suction side boundary layer thickens and develops pronounced turbulence at locations being closer to the TE. Therefore, the near-LE signatures of turbulent boundary layer noise disappear. 2) An extended multitude of peaks is present in the vicinity of the TE for each profile, near the profile surface. In the view that $\alpha = 10°$ relates to nearly maximum lift, mild near-TE flow separation is rendered possible. The peaks near the TE are assumed to be related to turbulent boundary layer noise and / or separated flow noise and / or trailing-edge noise and / or vortex-shedding noise.

$\alpha = 30°$. The peaks are located within the stalled zone for each profile. They are located not only in the vicinity of the profile but also farther away from it. No peaks are present in the vicinity of the TE. These peaks are assumed to be related to turbulent boundary layer noise and / or separated flow noise.

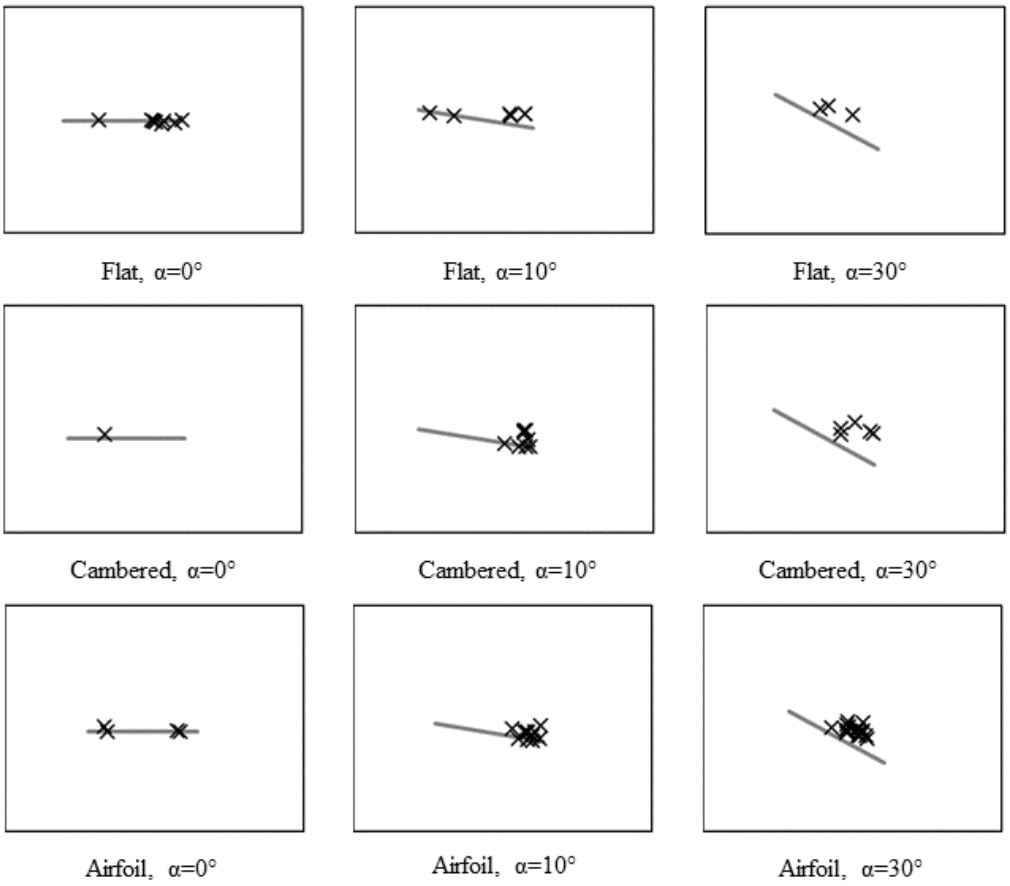

Figure 4. Loci of representative *SSL* peak values in the frequency range above 5 k *Hz*. The profiles are represented with their chord line.

5.2. Vortex shedding noise

Vortex shedding noise, presented in Figures 5 to 6, offers test cases for checking the reliability of the beamforming technique in finding the locus of a spatially distinct noise source. The Strouhal number characterizing the vortex shedding is defined herein as $St = f_S h/U$. For profile vortex shedding, the characteristic length scale h is the α–dependent height of the projection of the profile to the vertical $[y,z]$ plane (Yarusevych and Boutilier, 2010). For blunt trailing edge vortex shedding, h is the trailing edge thickness (Roger and Moreau, 2010). Yarusevych and Boutilier (2010)

published *St* values for various profiles, and for various α and *Re* values (including $\alpha = 10°$, and $Re = 1.4 \cdot 10^5$). On this basis, the Strouhal number valid for the profile vortex shedding cases, presented herein has briefly been estimated to $St \approx 0.8 \div 1$. In case of blunt trailing edge vortex shedding, *St* was presumed to be 0.2 on the basis of Roger and Moreau (2010). With knowledge of *U* as well as the actual *h* values, this enabled the selection of the third-octave bands within which the detection of vortex shedding noise is presumable. These bands have been selected as follows. Profile vortex-shedding noise: for $\alpha = 0°$: $f_{mid} = 2.5$ k*Hz* ("cambered", and "airfoil"); for $\alpha = 10°$: $f_{mid} = 1.25$ k*Hz* (each blade sections). Blunt trailing edge vortex shedding noise: for $\alpha = 0°$: $f_{mid} = 1.6$ k*Hz*, 2 k*Hz*, and 5 k*Hz*, for "flat", "cambered", and "airfoil", respectively. On the basis of the aforementioned references, no profile vortex shedding has been presumed for deep stall of $\alpha = 30°$, and no blunt trailing edge vortex shedding for $\alpha = 10°$ and $\alpha = 30°$.

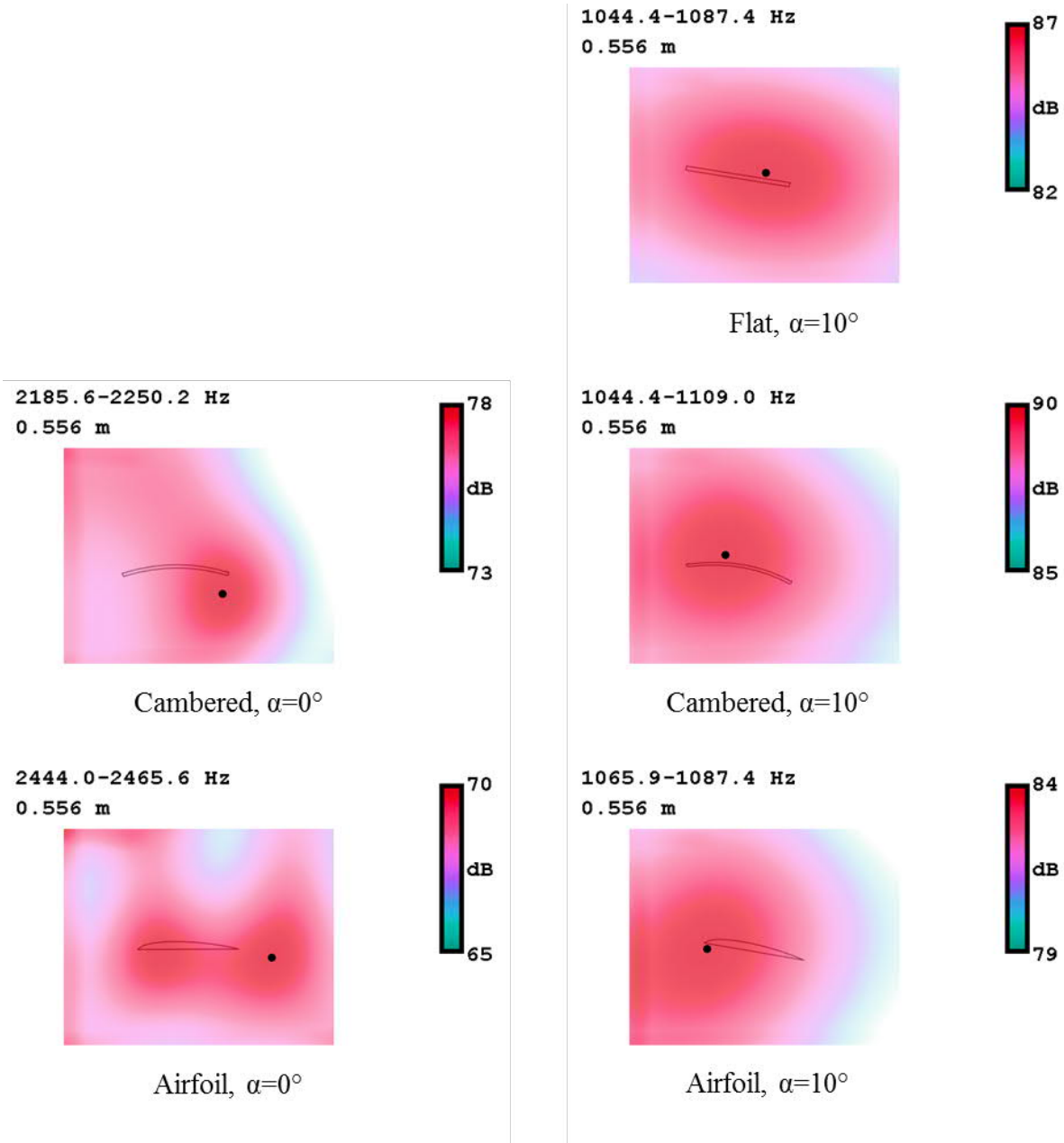

Figure 5. *SSL* [d*B*] source maps representing the presumed profile vortex-shedding noise. The black dot marks the position of the peak.

Considering the presumed vortex-shedding frequencies, the beamforming source maps within the aforementioned third-octave bands were systematically investigated for discovering the signatures of vortex-shedding noise. As the results of the investigation, Figures 5 and 6 present the source maps representing the presumed profile vortex-shedding noise and blunt trailing edge vortex-shedding noise, respectively. The contours of the profiles are illustrated in the diagrams. The presented frequency band is specified on the left-hand side above the individual diagrams. The black dots mark the location of the *SSL* peak within the frequency band.

As seen in the left column of Fig. 5, the beamforming technique localizes the source of presumed profile vortex-shedding noise to the vicinity of the TE at $\alpha = 0°$, in accordance with the expectation. (The map for the "flat" case is missing, since it is irrelevant for $\alpha = 0°$.) For $\alpha = 10°$ (right column), the peak has moved toward the upstream direction relative to the TE, for the "cambered" and "airfoil" cases. This suggests that the thickened suction side boundary layer at $\alpha = 10°$ provides an origin for profile vortex-shedding noise that is extended toward the region upstream of the TE. In the "airfoil" case at $\alpha = 10°$, the maximum is – erroneously – marked on the pressure side, indicating the limited spatial resolution of the PAM technique at lower frequencies. This case draws also the attention that the majority of profile vortex-shedding noise may originate from the vicinity of the LE of airfoils at increased angles of attack. The measurements by Yarusevych and Boutilier (2010) indicate that the laminar-to-turbulent transition in the separated shear layer occurs just at 15 to 20 percent chord downstream of the LE. It is presumed herein that such transition acts as the origin of profile vortex shedding noise.

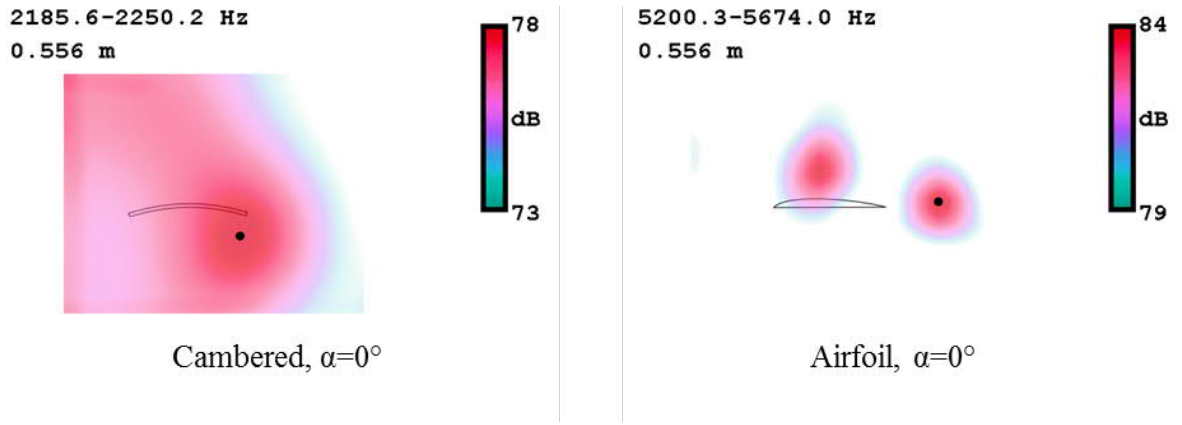

Figure 6. *SSL* [d*B*] source maps representing the presumed blunt trailing-edge vortex-shedding noise. The black dot marks the position of the peak.

Fig. 6 illustrates that, behaving as expected, the beamforming technique localizes the source of presumed blunt trailing edge vortex-shedding noise to the vicinity of the TE. For the flat plate, the blunt trailing edge vortex-shedding noise could not be distinguished with the processing technique presented herein. This necessitates the further improvement of the processing method.

Figs. 5 to 6 depict the following limitations in the presently available measurement and evaluation methodology. Upon need, these limitations are to be treated in the future research steps, by means of applying more sophisticated experimentation and / or data processing and evaluation.

Uncertainty in finding the locus of the dominant source. Examples: Fig. 5, "airfoil", $\alpha = 10°$: the peak is found on the pressure surface. Fig. 6, both case: the peak is not *exactly* at the TE.

Limits in spatial resolution. It is known that the resolving power is proportional with the frequency (e.g. Benedek and Vad, 2016). Examples: Fig. 5, each case: Although the dynamic range represented in these source maps remains the same as for Fig. 6, the moderate frequencies result in less contrasted (more blurry) *SSL* distribution. The zone of increased *SSL* extends in *x* and / or *z* direction.

Appearance of fake noise sources. Examples: Fig. 5, “cambered” and “airfoil” at α = 0°: increased level of fake noise appears in the region upstream of the profiles.

6. CONCLUSIONS AND FUTURE REMARKS

The paper illustrates the potential of the applied experimental technique in localizing the sources of blade section noise, such as turbulent boundary layer noise, separated flow noise, profile and blunt trailing edge vortex-shedding noise, and trailing-edge noise. The next steps are to carry out the comparative investigation for lower Reynolds numbers, e.g. $Re = 6 \cdot 10^4$, and to establish a quantitative model for the noise of cambered plates. These steps will contribute to design of low-noise, low-Reynolds-number axial fans equipped with cambered plate blades. The following limitations of the experimental technique, as well as of the data processing and evaluation method, are acknowledged, and are to be treated / considered in future work: neglect of mean flow deviation; limit in the validity of the 2D approach; high background noise; spatial uncertainty of source localization; limits in spatial resolution; appearance of fake noise sources.

ACKNOWLEDGEMENTS

This work has been supported by the Hungarian National Fund for Science and Research under contracts NKFI K 112277. The work relates to the scientific programs "Development of quality-oriented and harmonized R+D+I strategy and the functional model at BME" (Project ID: TÁMOP-4.2.1/B-09/1/KMR-2010-0002) and "Talent care and cultivation in the scientific workshops of BME" (Project ID: TÁMOP-4.2.2/B-10/1-2010-0009).

REFERENCES

Albring, W. (1978), *Angewandte Strömungslehre*. 6., bearbeitete Auflage. Akademie-Verlag Berlin, 1978/1990.

Balla, E., Vad, J. (2017), Establishment of a beamforming dataset on basic models of low-speed axial fan blade sections. *Periodica Polytechnica, Mechanical Engineering* (to appear)

Benedek, T., Vad, J. (2016), An industrial on-site methodology for combined acoustic-aerodynamic diagnostics of axial fans, involving the phased array microphone technique. *Int. J. Aeroacoustics*, **15**, pp. 81-102.

Borges, S. S. (2012), CFD techniques applied to axial fans design of electric motors. *Proc. International Conference on Fan Noise, Technology and Numerical Methods (FAN2012)* , Senlis, France.

Brooks, T. F., Pope, D. S., Marcolini, M. A. (1989), Airfoil self-noise and prediction. *NASA Reference Publication* 1218.

Carolus, T. (2003), *Ventilatoren*. B. G. Teubner Verlag, Wiesbaden.

Corsini, A., Rispoli, F. (2004), Using sweep to extend the stall-free operational range in axial fan rotors. *Proc. Instn Mech. Engrs, Part A, J. Power and Energy* , **218**, pp. 129-139.

Daly, B. B. (1992), *Woods practical guide to fan engineering* . Woods of Colchester Ltd. (sixth impression)

Dougherty, R. P. (2002), *Beamforming in acoustic testing*, in: T. J. Mueller (Ed.), Experimental Aeroacoustics, Springer, Berlin, 2002, pp. 62-97.

Dougherty, R. P. (2016), Cross spectral matrix diagonal optimization. *BeBec Paper 2016-S2*.

Geyer, T., Sarradj, E., Giesler, J. (2012), Application of a beamforming technique to the measurement of airfoil leading edge noise. *Advances in Acoustics and Vibration*, Volume 2012, Article ID 905461.

Gue, F., Cheong, C., Kim, T. (2011), Development of low-noise axial cooling fans in a household refrigerator. *J. Mechanical Science and Technology* , **25**, pp. 2995-3004.

Gulyás, A., Balczó, M. (2014), Development of a small blower-type wind tunnel for educational purposes. *28th microCAD International Multidisciplinary Scientific Conference,* Miskolc, Hungary (ISBN:978-963-358-051-6)

Herold, G., Sarradj, E. (2015), Microphone array method for the characterization of rotating sound sources in axial fans. *Proc. International Conference on Fan Noise, Technology and Numerical Methods (FAN2015)*, Lyon, France.

Horváth, Cs. (2015), Beamforming investigation of dominant counter-rotating open rotor tonal and broadband noise sources. *AIAA Journal*, **53**, pp. 1602-1611.

Huang, L. X. (2003), Characterizing computer cooling fan noise. *J. Acoust. Soc. Am.*, **114**, pp. 3189-3200.

Hutcheson, F. V., Brook, T. F. (2006), Effects of angle of attack and velocity on trailing edge noise determined using microphone array measurements. *Int. J. Aeroacoustics*, **5**, pp. 39-66.

Koop, L. (2006), *Beamforming in acoustic testing*, in: M. L. Riethmuller, M. R. Lena (Eds.), VKI Experimental Aeroacoustics, von Kármán Institute for Fluid Dynamics, Rhode Saint Genese, 2006.

Mckinzie, D. J., Burns, R. J. (1975), Analysis of noise produced by jet impingement near the trailing edge of a flat and a curved plate. *NASA Technical Memorandum* NASA TM X-3171.

Minck, O., Binder, N., Cherrier, O., Lamotte, L., Budinger, V. (2012), Fan noise analysis using a microphone array. *Proc. International Conference on Fan Noise, Technology and Numerical Methods (FAN2012)*, 18-20 April 2012, Senlis, France.

Moreau, D. J., Doolan, C. J. (2016), Tonal noise production from a wall-mounted finite airfoil. *J. Sound and Vibration*, **363**, pp. 199-224.

Moreau, D. J., Doolan, C. J., Alexander, W. N., Meyers, T. W., Devenport, W. J. (2016), Wall-mounted finite airfoil-noise production and prediction. *AIAA Journal*, **54**, pp. 1637-1651.

Mueller, T. J. (1999), Aerodynamic measurements at low Reynolds numbers for fixed wing micro-air vehicles. *RTO AVT/VKI Special Course, Development and operation of UAVs for military and civil applications*, 13-17 September 1999, VKI, Belgium.

Padois, T., Laffay, P., Idier, A., Moreau, S. (2015), Detailed experimental investigation of the aeroacoustic field around a controlled-diffusion airfoil. *AIAA Paper* 2015-2205.

Padois, T., Laffay, P., Idier, A., Moreau, S. (2016), Tonal noise of a controlled-diffusion airfoil at low angle of attack and Reynolds number. *J. Acoust. Soc. Am.*, **140**, pp. EL113-EL118.

Patterson, G. N. (1944), Ducted fans. Design for high efficiency. *Australian Council for Aeronautics Report* ACA 7.

Pelletier, A., Mueller, T. J. (2000), Low Reynolds number aerodynamics of low-aspect ratio, thin/flat/cambered-plate wings. *J. Aircraft*, **37**, pp. 825-832.

Roger, M., Moreau, S. (2010), Extensions and limitations of analytical airfoil broadband noise models. *Int. J. Aeroacoustics*, **9**, pp. 273-305.

Staubs, J. K. (2008), Real airfoil effects on leading edge noise. *Ph.D. Thesis*, Virginia Polytechnic Institute and State University, Blacksburg, VA.

Sturm, M., Sanjosé, M., Moreau, S., Carolus, T. (2015), Application of analytical noise models using numerical and experimental fan data. *Proc. 11th European Conference on Turbomachinery Fluid Dynamics and Thermodynamics (ETC'11)*, Madrid, Spain.

Vad, J., Koscsó, G., Gutermuth, M., Kasza, Zs., Tábi, T., Csörgő, T. (2006), Study of the aero-acoustic and aerodynamic effects of soft coating upon airfoil. *JSME Int. J. Series C-Mechanical Systems Machine Elements and Manufacturing*, **49**, pp. 648-656.

Vad, J., Horváth Cs., Kovács J.G. (2014), Aerodynamic and aero-acoustic improvement of electric motor cooling equipment. *Proc. Instn Mech. Engrs, Part A, J. Power and Energy*, **228**, pp. 300-316.

VDI Richtlinie 3731 (1990), Emissionskennwerte technischer Schallquellen / Ventilatoren. Blatt 2.

Wallis, R. A. (1946), Wind tunnel tests on a series of circular arc plate aerofoils. *A.R.L. Aero Note* 74.

Yarusevych, S., Boutilier, M. S. H. (2010), Vortex shedding characteristics of a NACA 0018 Airfoil at low Reynolds numbers. *AIAA Paper* 2010-4628.

Zenger, F., Herold, G., Becker, S. (2016), Acoustic characterization of forward- and backward-skewed axial fans under increased inflow turbulence. *AIAA Paper* 2016-2943.